OPEN

Efficient NH₃-based process to remove chlorine from electron beam deposited ruthenium produced from $(\eta^3\text{-}C_3H_5)Ru(CO)_3Cl$

Markus Rohdenburg [1]✉, Hannah Boeckers[1], Christopher R. Brewer [2], Lisa McElwee-White [2] & Petra Swiderek[1]✉

The fabrication of Ru nanostructures by focused electron beam induced deposition (FEBID) requires suitable precursor molecules and processes to obtain the pure metal. So far this is problematic because established organometallic Ru precursors contain large organic ligands, such as cyclopentadienyl anions, that tend to become embedded in the deposit during the FEBID process. Recently, $(\eta^3\text{-}C_3H_5)$ $Ru(CO)_3X$ (X = Cl, Br) has been proposed as an alternative precursor because CO can easily desorb under electron exposure. However, allyl and Cl ligands remain behind after electron irradiation and the removal of the halide requires extensive electron exposures. Auger electron spectroscopy is applied to demonstrate a postdeposition purification process in which NH₃ is used as a reactant that enhances the removal of Cl from deposits formed by electron irradiation of thin condensed layers of $(\eta^3\text{-}C_3H_5)$ $Ru(CO)_3Cl$. The loss of CO from the precursor during electron-induced decomposition enables a reaction between NH₃ and the Cl ligands that produces HCl. The combined use of electron-stimulated desorption experiments and thermal desorption spectrometry further reveals that thermal reactions contribute to the loss of CO in the FEBID process but remove only minor amounts of the allyl and Cl ligands.

Focused electron beam induced deposition (FEBID) is a state-of-the art nanofabrication process, capable of producing freestanding nanometer-sized structures with arbitrary shape[1–4]. In FEBID, precursor molecules adsorbed on a surface are decomposed under a tightly focused high-energy electron beam to produce the desired solid material. Deposition of a particular metal thus requires a suitable organometallic precursor. Ideally, this precursor should decompose completely upon electron irradiation to leave only the metal behind, while the ligands are efficiently converted to volatile byproducts that desorb from the deposit. However, metallic nanostructures produced by FEBID are often contaminated by considerable amounts of unwanted elements from incomplete ligand desorption, so that the targeted properties are not achieved[1,5–7]. Therefore, many common FEBID precursors require strategies to purify the deposit[5].

A wide variety of purification strategies for FEBID has been reported, including thermal reactions, prolonged electron exposure, process gases, or a combination of at least two of these approaches[5]. A recent successful development is to use H_2O as process gas[8,9]. For instance, carbon-rich deposits produced from trimethyl(methylcyclopentadienyl)platinum(IV) (MeCpPtMe₃) were converted to pure Pt by post-deposition electron irradiation in the presence of H_2O[8]. As another example, a FEBID process that simultaneously dosed dimethyl(acetylacetonato)gold(III) (AuMe₂(acac)) and H_2O yielded a deposit with Au content above 80%, in contrast to low-purity deposits produced from AuMe₂(acac) alone[9]. A study of such processes in the case of MeCpPtMe₃ by surface science techniques showed that H_2O converts the carbon content to CO and CH₄[10].

An important application of FEBID is the repair of masks for photolithography[11,12]. In this area, the emerging nanofabrication tool extreme ultraviolet lithography (EUVL), requires capping layers that protect the masks during processing and exposure. Ru has been identified as a material of choice for this purpose[11]. Therefore, FEBID processes that yield high purity Ru are of interest for EUVL mask repair. However, the best commonly

¹Institute for Applied and Physical Chemistry (IAPC), Fachbereich 2 (Chemie/Biologie), University of Bremen, Leobener Str. 5 (NW2), 28359 Bremen, Germany. ²Department of Chemistry, University of Florida, Gainesville, FL 32611-7200, USA. ✉email: m.rohdenburg@uni-bremen.de; swiderek@uni-bremen.de
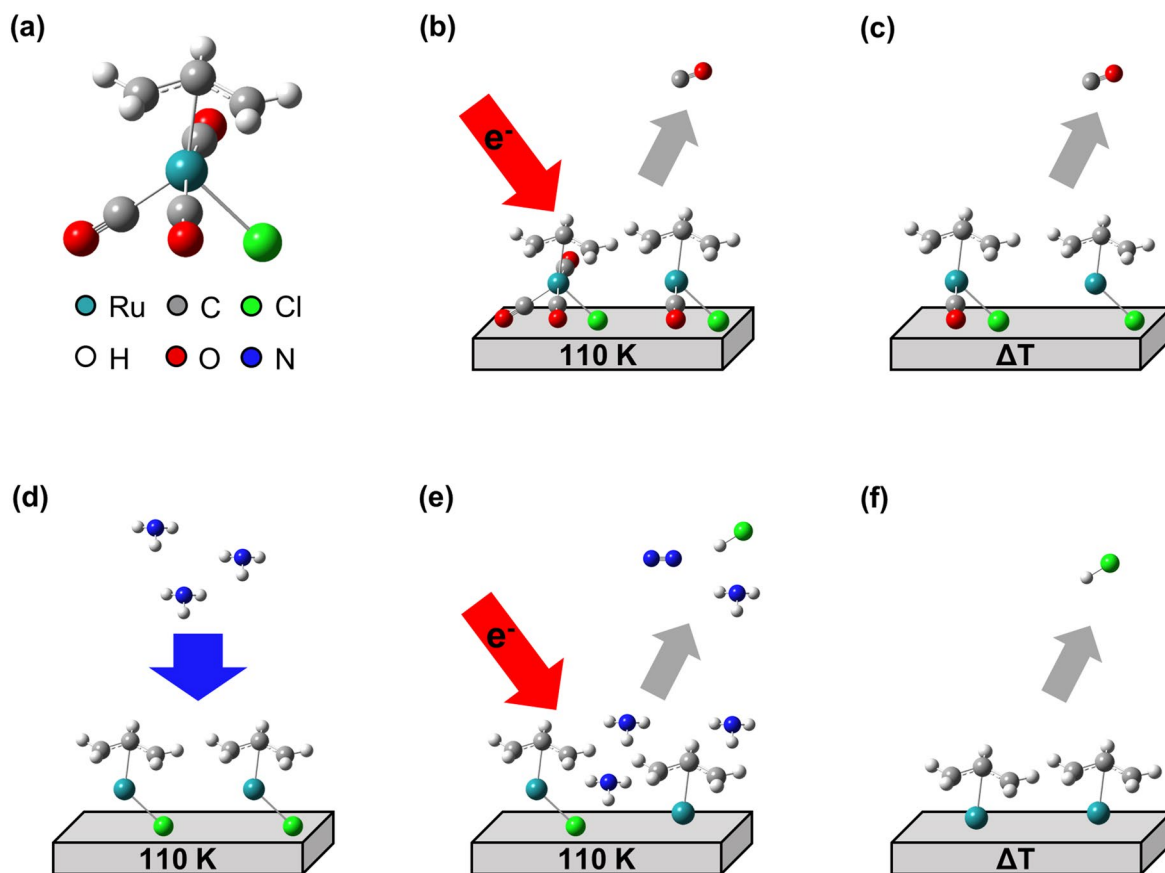
Figure 1. Overview of experiments to unravel the chemistry that underlies the electron-induced formation of deposits from the Ru precursor $(\eta^3\text{-}C_3H_5)Ru(CO)_3Cl$ and the NH_3-assisted purification process aiming at removal of Cl from the deposits. **(a)** Structure of the precursor and colour scheme of the relevant elements. Deposits were produced by **(b)** electron-stimulated desorption (ESD) from thin condensed layers of $(\eta^3\text{-}C_3H_5)Ru(CO)_3Cl$ on Ta held at 110 K and **(c)** subsequent thermal desorption spectrometry (TDS) during which the sample was annealed to 450 K at a rate of 1 K/s. The deposit was used in the subsequent purification experiments consisting of several cycles in each of which **(d)** NH_3 was condensed onto the deposit at 110 K, followed by **(e)** an ESD and **(f)** a TDS experiment. Desorption of volatile species was monitored in all experiments by mass spectrometry (MS).

used precursor for Ru, bis(ethylcyclopentadienyl)ruthenium(II) $((EtCp)_2Ru)$ retains large amounts of carbon during its electron-induced decomposition, while removal of carbon from the deposit by electron irradiation in the presence of O_2 results in oxidation of the metal[11]. Novel precursors for FEBID processes aiming at pure Ru deposits are of interest to address these challenges. Therefore, a class of Ru precursors, namely η^3-allyl ruthenium tricarbonyl halides $((\eta^3\text{-}C_3H_5)Ru(CO)_3X, X = Cl, Br)$, has been proposed and its electron-induced chemistry has been studied in the gas-phase[13] and on surfaces[14]. Also, the performance of $(\eta^3\text{-}C_3H_5)Ru(CO)_3Br$ in the FEBID process was investigated[15]. The advantage of these precursors lies in the lower number of carbon atoms as compared to $(EtCp)_2Ru$. Additionally, the CO ligands, which contribute half of the carbon content in the precursor, are particularly facile to remove. However, extensive electron irradiation is required to remove the halide ligand[14].

We have recently studied the electron-induced decomposition of cisplatin $(cis\text{-}Pt(NH_3)_2Cl_2)$ and shown that its NH_3 ligands assist with the removal of Cl from the resulting deposit[16,17]. Under electron exposure, the NH_3 ligands decompose to deliver hydrogen that converts the Cl ligands to volatile HCl[16]. Herein, we show that this reducing action of NH_3 can also be exploited to purify deposits produced from thin condensed layers of $(\eta^3\text{-}C_3H_5)Ru(CO)_3Cl$ (Fig. 1a) by electron irradiation at cryogenic temperature (Fig. 1b) and subsequent annealing (Fig. 1c). The chemistry underlying the purification process was studied by repeatedly condensing NH_3 on the cold deposit (Fig. 1d) followed by electron irradiation (Fig. 1e) and a further annealing step (Fig. 1f). During irradiation sequences, the electron-stimulated desorption (ESD) of volatile products was monitored. Thermal desorption spectrometry (TDS) performed during the annealing steps revealed not only products that were formed during electron irradiation and desorb at higher temperature, but also products resulting from thermal reactions that set in above specific temperatures. Furthermore, reflection absorption infrared spectroscopy (RAIRS) monitored the remaining CO ligands after electron exposure and annealing. As introduced recently[10], the combination of ESD and TDS allows us to identify contributions of thermal reactions to the electron-induced chemistry involved in FEBID. This bridges the gap between the previous surface science studies[14] and the actual FEBID experiments[15] on $(\eta^3\text{-}C_3H_5)Ru(CO)_3X$ precursors. Using Auger electron spectroscopy (AES), we then
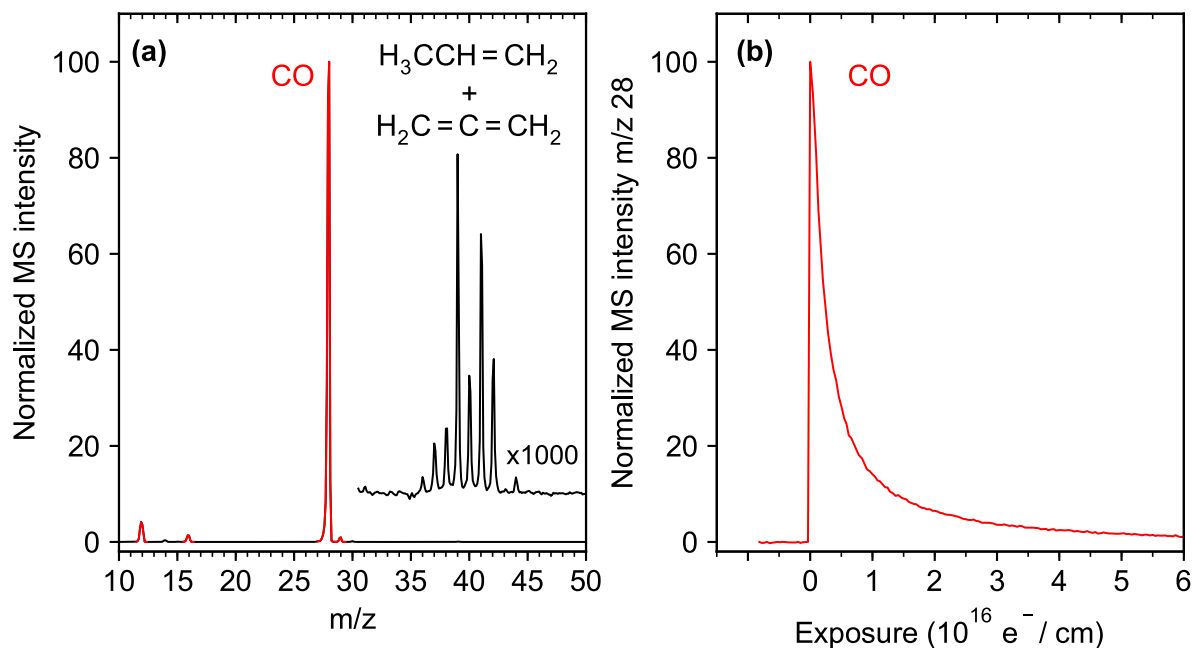
Figure 2. Electron-stimulated desorption (ESD) data obtained during electron exposure at $E_0 = 31$ eV from an adsorbed layer of $(\eta^3$-C$_3$H$_5)$Ru(CO)$_3$Cl on Ta held at 110 K. **(a)** Mass spectrum recorded during the initial stage of electron exposure and blow-up of the spectrum above m/z 30. **(b)** Decay of CO signal (m/z 28) as function of electron exposure. The total exposure of this experiment amounted to $1.25\cdot10^{17}$ e$^-$/cm^2 and the sample current dropped slightly from $I_p = 100$ μA to 96 μA during the entire irradiation period.

provide evidence that NH$_3$ is in fact a suitable process reagent to remove Cl, and potentially also other halides during FEBID processes using halide containing precursors.

Results

Electron-stimulated desorption from adsorbed $(\eta^3$-C$_3$H$_5)$Ru(CO)$_3$Cl.
The electron-induced degradation of thin $(\eta^3$-C$_3$H$_5)$Ru(CO)$_3$Cl layers on Ta was studied at 110 K by monitoring ESD of volatile products as visualized in Fig. 1b. A representative data set is shown in Fig. 2. In line with previous results[14], only CO was detected with noticeable intensity during irradiation, as indicated by the signals at m/z 28, m/z 16 and m/z 12 in the mass spectrum (Fig. 2a). Very small signals in the range m/z 36–42 become visible when the spectrum is blown up by a factor of 1,000 (range above m/z 30 in Fig. 2a), which is characteristic of hydrocarbon compounds with three carbon atoms (C$_3$ hydrocarbons), such the allyl ligands of $(\eta^3$-C$_3$H$_5)$Ru(CO)$_3$Cl. Our ESD experiments detect neutral species for which the desorption cross sections are at least an order of magnitude higher than for ions[18], with the majority of products being stable neutral species[10,16]. However, the intensity pattern observed here matches neither the mass spectrum of propene (H$_2$C = CH-CH$_3$) nor that of propadiene (H$_2$C = C = CH$_2$) (compare mass spectra in[19]). Propene and propadiene would both derive from H-abstraction processes involving an allyl radical. In the case of propene, C1 or C3 of the allyl radical abstracts H from another species. Propadiene would arise from loss of the C2 hydrogen from an allyl radical. However, by overlaying both mass spectra weighted by suitable factors, the mass spectrum observed during ESD is roughly reproduced (Supplementary Information, Fig. S1), suggesting that H transfer occurs as a minor reaction channel. Note that Cl (m/z 35) is absent from the mass spectrum acquired during electron exposure.

The m/z 28 signal decayed during irradiation and nearly ceased after an electron exposure of $6\cdot10^{16}$ e$^-$/cm^2 (Fig. 2b). We note that ESD of CO during the present experiments at 31 eV decayed on a similar time scale as previously observed for a layer of the related compound, $(\eta^3$-C$_3$H$_5)$Ru(CO)$_3$Br, on Au with a similar thickness (stated as 1–2 nm), but irradiated at 500 eV[14]. This is surprising regarding previous results for cisplatin which decomposed much more rapidly at 500 eV than at 50 eV within the same electron exposure[16]. Notably, the different halogen does not appear to affect the decomposition rate of the Ru precursors because the loss of CO proceeded at a similar rate for $(\eta^3$-C$_3$H$_5)$Ru(CO)$_3$Br and $(\eta^3$-C$_3$H$_5)$Ru(CO)$_3$Cl according to XPS[14]. We can also exclude charging of the samples in our experiment as origin of the rapid decay of ESD because the sample current was nearly constant during the entire irradiation period. Additionally, an effect of the different underlying metal is unlikely because the secondary electron (SE) yields are similar for Ta and Au[20], so that it is not conceivable that more SEs should be produced at 31 eV from Ta in the present experiment than at 500 eV from Au as used previously[14]. Therefore, the rapid decomposition of $(\eta^3$-C$_3$H$_5)$Ru(CO)$_3$Cl at 31 eV must be an inherent property of the precursor.

Post-irradiation thermal desorption from adsorbed $(\eta^3$-C$_3$H$_5)$Ru(CO)$_3$Cl.
Following the complete decay of the CO signal in ESD from the freshly prepared precursor layer, a post-irradiation TDS experiment was
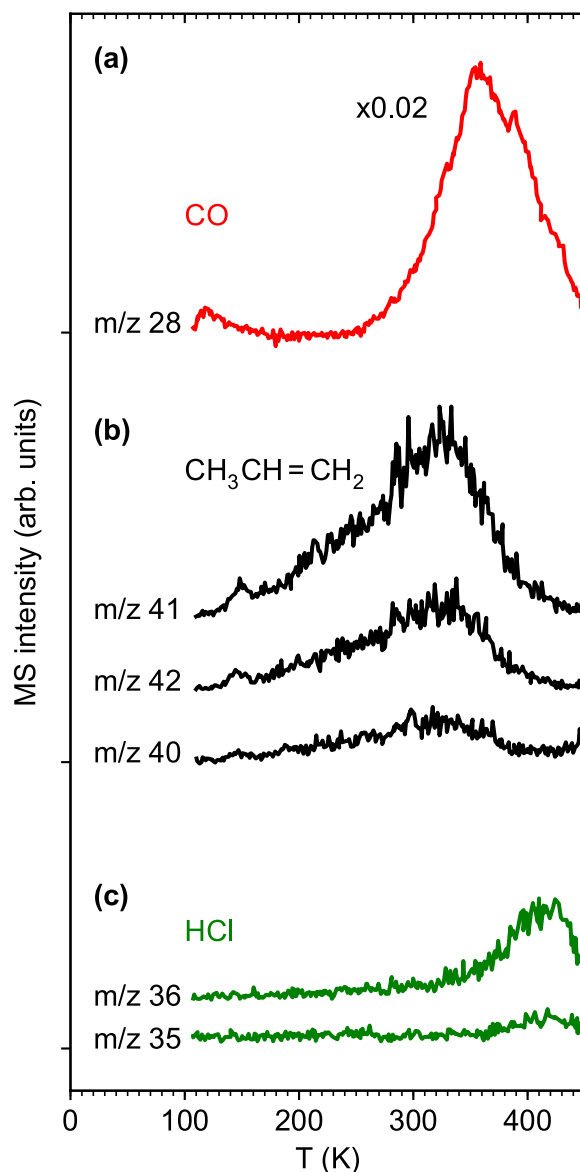
Figure 3. Thermal desorption spectra (TDS) acquired from an adsorbed layer of $(\eta^3\text{-}C_3H_5)Ru(CO)_3Cl$ on Ta following an electron exposure of $1.25 \cdot 10^{17}$ e$^-$/cm^2 at $E_0 = 31$ eV. The selected m/z values give evidence of desorption of **(a)** CO, **(b)** propene, and **(c)** HCl.

performed on each sample (see Fig. 1c). Figure 3 shows a representative result. Here, m/z 41 gives evidence that $(\eta^3\text{-}C_3H_5)Ru(CO)_3Cl$ has in fact been mainly decomposed as the characteristic desorption peak near 220 K of the intact precursor (Supplementary Information, Fig. S2) is absent after electron exposure. In contrast, a broad signal with onset near 150 K and maximum around 300 K is present in the m/z 41 TDS curve after irradiation. Desorption signals with the same shape and maximum are seen in the m/z 40 and m/z 42 data. The relative intensities of these three signals agree well with the mass spectrum of propene (m/z 42 (70%), 41 (100%), 40 (30%)[19]). Physisorbed propene desorbs well below 100 K[21] so that it should have evaporated at least partially if it had formed during electron irradiation which proceeded at 110 K. The fact that the observed product propene desorbs at a much higher temperature according to TDS indicates that it is formed not as an immediate consequence of electron irradiation but that a thermally activated reaction step must be involved.

Desorption of HCl with onset above 300 K and maximum above 400 K is evident from TDS data recorded at m/z 36 and m/z 35 and supported by the mass spectrum of HCl (m/z 36 (100%), 35 (18%)[19]). Similar desorption temperatures, i.e., a signal between 300 and 350 K, have been observed for HCl on Pt(111) at the lowest coverage[22], and desorption of HCl from a single crystal alumina surface started around 300 K and peaked just below 400 K[23]. However, physisorbed HCl would again desorb below 100 K[22]. Consequently, the absence of signals at m/z 35 and m/z 36 in ESD (Fig. 2) supports that thermal activation is required to release HCl to the gas phase.
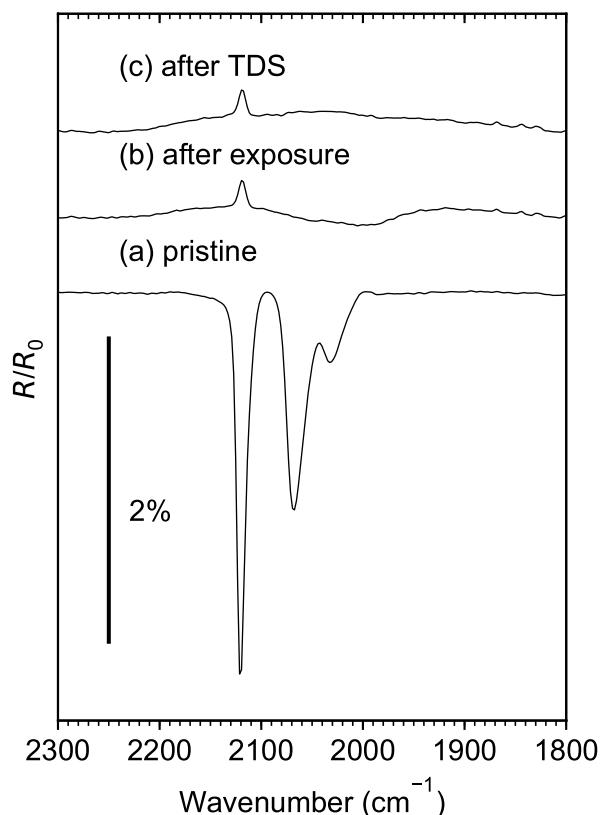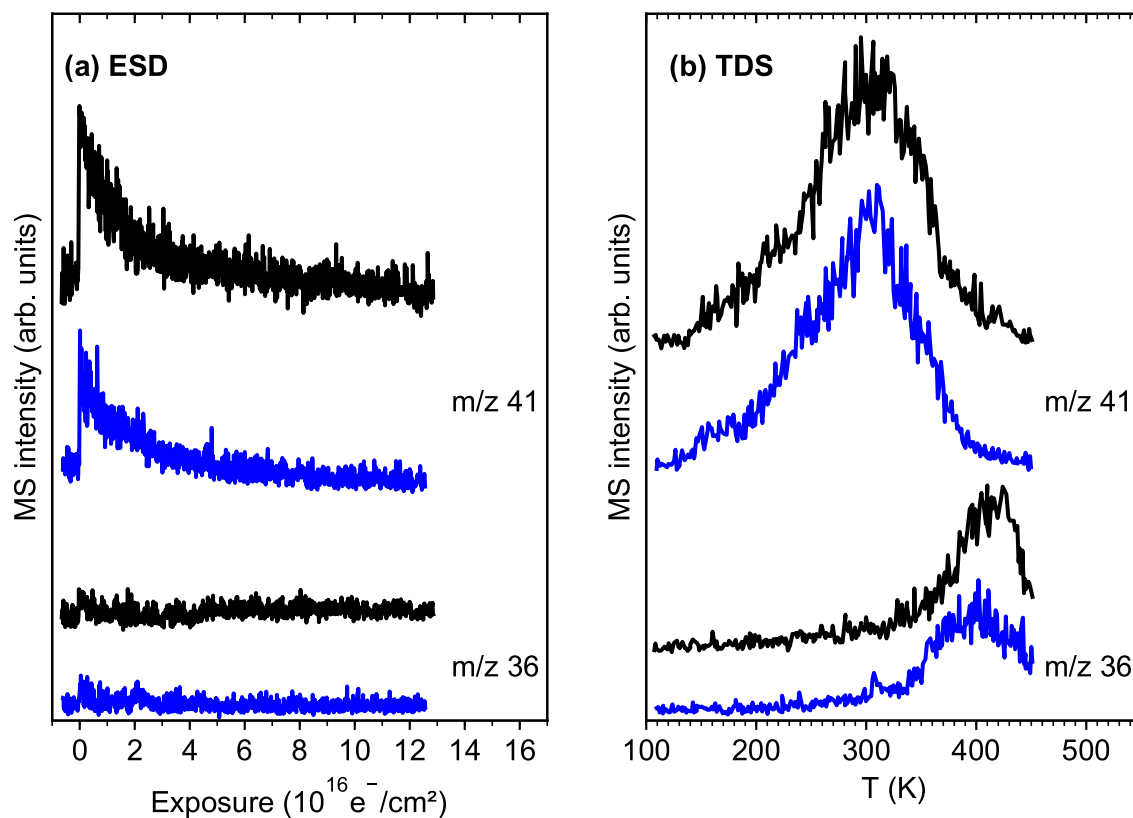
Figure 4. **(a)** Reflection absorption infrared spectrum (RAIRS) acquired on a pristine adsorbed layer of (η^3-C$_3$H$_5$)Ru(CO)$_3$Cl on Ta. **(b)** RAIRS of the same layer after an electron exposure of $1.25 \cdot 10^{17}$ e$^-$/cm^2 at $E_0 = 31$ eV. **(c)** RAIRS of the same layer after annealing to 450 K during a subsequent TDS experiment and final cooling to 110 K.

Finally, an intense signal with onset near 300 K and maximum around 360 K is present in the TDS curve for m/z 28. It is assigned to desorption of additional CO as confirmed by a mass spectrum acquired near 360 K in a separate experiment and revealing the absence of other products such as hydrocarbons or CO$_2$ (m/z 44) (Supplementary Information, Fig. S3). The high temperature supports the release of CO through a thermal surface reaction.

Based on tabulated total ionization cross sections for CO, propene, and HCl[24,25], and the fragmentation pattern of the mass spectra[19], the partial ionization cross sections for the formation of CO$^+$ from CO, C$_3$H$_5$$^+$ from propene, and HCl$^+$ from HCl can be derived as σ_{BEB}(CO, m/z 28) = 2.35 Å^2, σ_{BEB}(propene, m/z 41) = 2.21 Å^2, and σ_{BEB}(HCl, m/z 36) = 3.53 Å^2. The intensities observed for CO at m/z 28 and propene at m/z 41 in the present TDS experiments thus reflect approximately the relative amounts of these two products. Accordingly, propene seen in post-irradiation TDS amounts to roughly 2% of the quantity of CO released through thermal processing. Together with the even smaller hydrocarbon desorption signals during ESD as compared to CO (Fig. 2a), our results indicate that most of the allyl carbon is retained in the deposit. This information was obscured in previous XPS results by the strong overlap of the C 1 s and Ru 3d signals[14] but evidence for a large amount of residual carbon was seen in the nanogranular structure of FEBID deposits fabricated from (η^3-C$_3$H$_5$)Ru(CO)$_3$Br[15]. The even smaller desorption signal at m/z 36 together with the larger partial ionization cross section for the parent ion of HCl further indicates that the quantity of HCl that desorbs during annealing (Fig. 3) following electron exposure of $1.25 \cdot 10^{17}$ e$^-$/cm^2 (Fig. 2) is even smaller (< 1%). This estimate is in line with the previous result that most of the Cl content was retained on the surface after a similar electron exposure ($8 \cdot 10^{16}$ e$^-$/cm^2) of (η^3-C$_3$H$_5$)Ru(CO)$_3$Cl at 105 K and 500 eV[14].

The relative amounts of CO released during electron irradiation and subsequent thermal desorption has been evaluated from the areas under the ESD and TDS curves recorded for m/z 28. As a result, the amount of CO that desorbs during electron exposure at 110 K exceeds the amount observed in TDS by a factor of roughly nine. This is close to the previously reported CO signal in XPS that decayed to roughly 20% of the initial intensity after a similar electron exposure ($8 \cdot 10^{16}$ e$^-$/cm^2) at 500 eV[14], pointing again to the surprising efficiency of CO removal at 31 eV.

Loss of CO monitored by reflection–absorption infrared spectroscopy. To monitor CO that remains on the surface even after thermal treatment, RAIRS experiments were performed on a pristine layer of (η^3-C$_3$H$_5$)Ru(CO)$_3$Cl, the same layer after the ESD experiment, and after subsequent TDS (Fig. 4), i.e., before
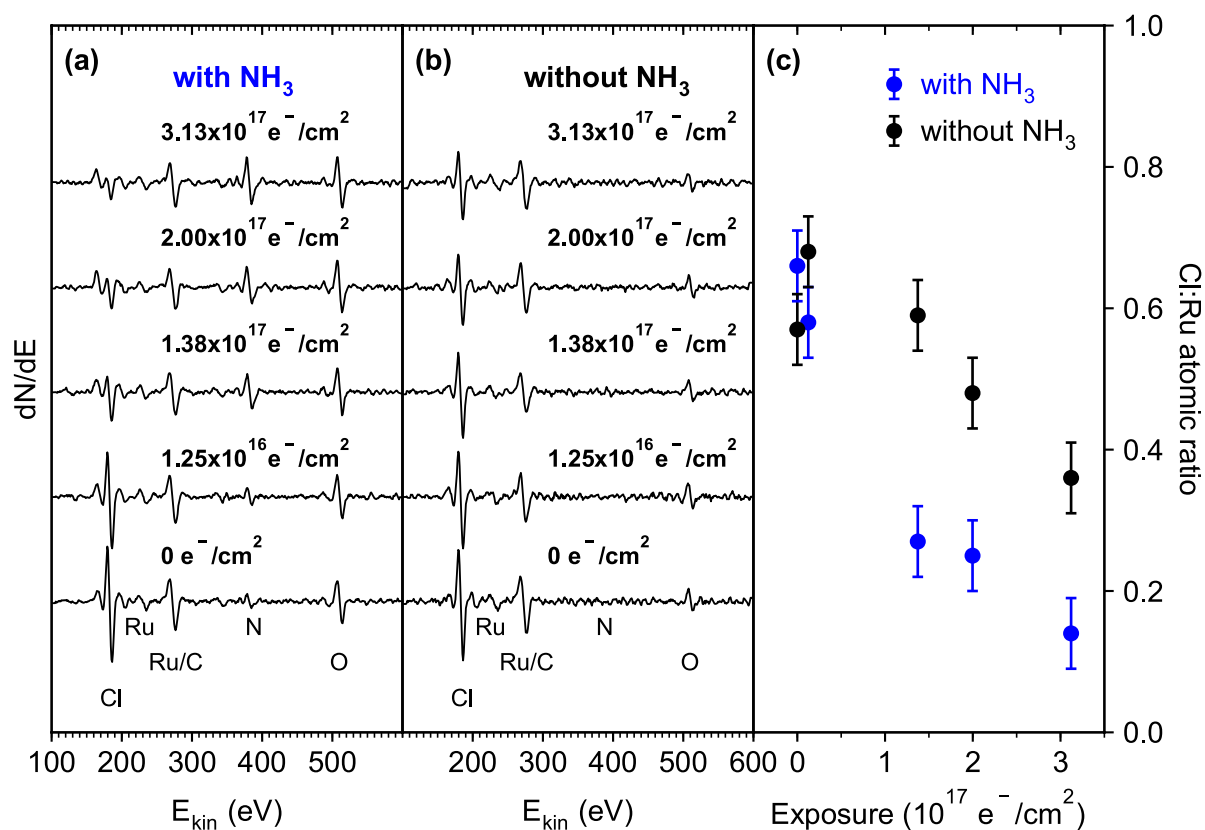
Figure 5. (**a**) Electron-stimulated desorption (ESD) signals at *m/z* 41 (C$_3$ hydrocarbon) and *m/z* 36 (HCl) recorded during an electron exposure of 1.25·10^{17} e$^-$/cm^2 at $E_0 = 31$ eV of (η^3-C$_3$H$_5$)Ru(CO)$_3$Cl on Ta held at 110 K. (**b**) Thermal desorption spectra (TDS) recorded following the same ESD experiments. The data plotted in black refer to an experiment performed in the absence of NH$_3$ while the precursor layer was covered by NH$_3$ in the case of the data plotted in blue.

and after the experimental steps visualized by Fig. 1b and c. The pristine layer (Fig. 4a) shows three intense CO stretching bands in line with a previous ATR-IR result[14] but somewhat shifted to 2,122 cm^{-1}, 2,072 cm^{-1}, and 2,034 cm^{-1}. These bands have disappeared after the ESD experiment leaving behind a broad band around 1990 cm^{-1} (Fig. 4b). This band coincides with the band positions of CO on Ru(0001) at low coverage[26]. Considering that the loss of CO during electron exposure proceeded simultaneously with reduction of the Ru center from Ru(II) to a state closer to metallic Ru[14], we tentatively assign the broad band around 1990 cm^{-1} to CO that remains attached to such reduced metal sites. This signal has, however, disappeared after the TDS experiment (Fig. 4c) indicating that the thermal treatment, in fact, removed all residual CO.

Electron-stimulated desorption from adsorbed (η^3-C$_3$H$_5$)Ru(CO)$_3$Cl in presence of NH$_3$. In a control experiment, NH$_3$ was condensed on top of a pristine layer of (η^3-C$_3$H$_5$)Ru(CO)$_3$Cl to assess if its presence enhances the removal of Cl from the precursor. Again, a combined ESD and TDS experiment was performed under the same conditions as described in the previous section. Figure 5 shows that the desorption signals for *m/z* 41 (C$_3$ hydrocarbons) and *m/z* 36 (HCl) obtained with and without NH$_3$ are very similar. In particular, an enhancement of the HCl production in presence of NH$_3$ is clearly not observed.

We note that the temperature in the present experiments was close to the multilayer desorption temperature of NH$_3$ as observed in experiments performed at lower temperature[21] (see also "Methods"). Therefore, a TDS experiment was performed without prior electron exposure to verify that some NH$_3$ actually sticks on the preadsorbed precursor layer. In fact, a desorption signal of NH$_3$ set in sharply at the start of the temperature ramp and leveled off slowly to extend up to the desorption temperature of the precursor supporting adsorption of NH$_3$ (Supplementary Information, Fig. S4). Consequently, the absence of enhanced HCl production (Fig. 5) demonstrates that NH$_3$ does not efficiently react with (η^3-C$_3$H$_5$)Ru(CO)$_3$Cl upon electron exposure.

Deposit purification by electron irradiation in presence of NH$_3$ monitored by Auger electron spectroscopy. In the set of experiments aiming at the deposit purification process, we investigated the efficiency of NH$_3$ with respect to removal of Cl from a deposit prepared from (η^3-C$_3$H$_5$)Ru(CO)$_3$Cl by the sequence of ESD and TDS experiments described above (see Fig. 1b and c). A total of 25 purification cycles were performed on the deposit. In each cycle, NH$_3$ was condensed on the deposit at 110 K (see Fig. 1d) and an electron exposure of 1.25·10^{16} e$^-$/cm^2 was applied at 31 eV during which ESD data were recorded (see Fig. 1e), followed
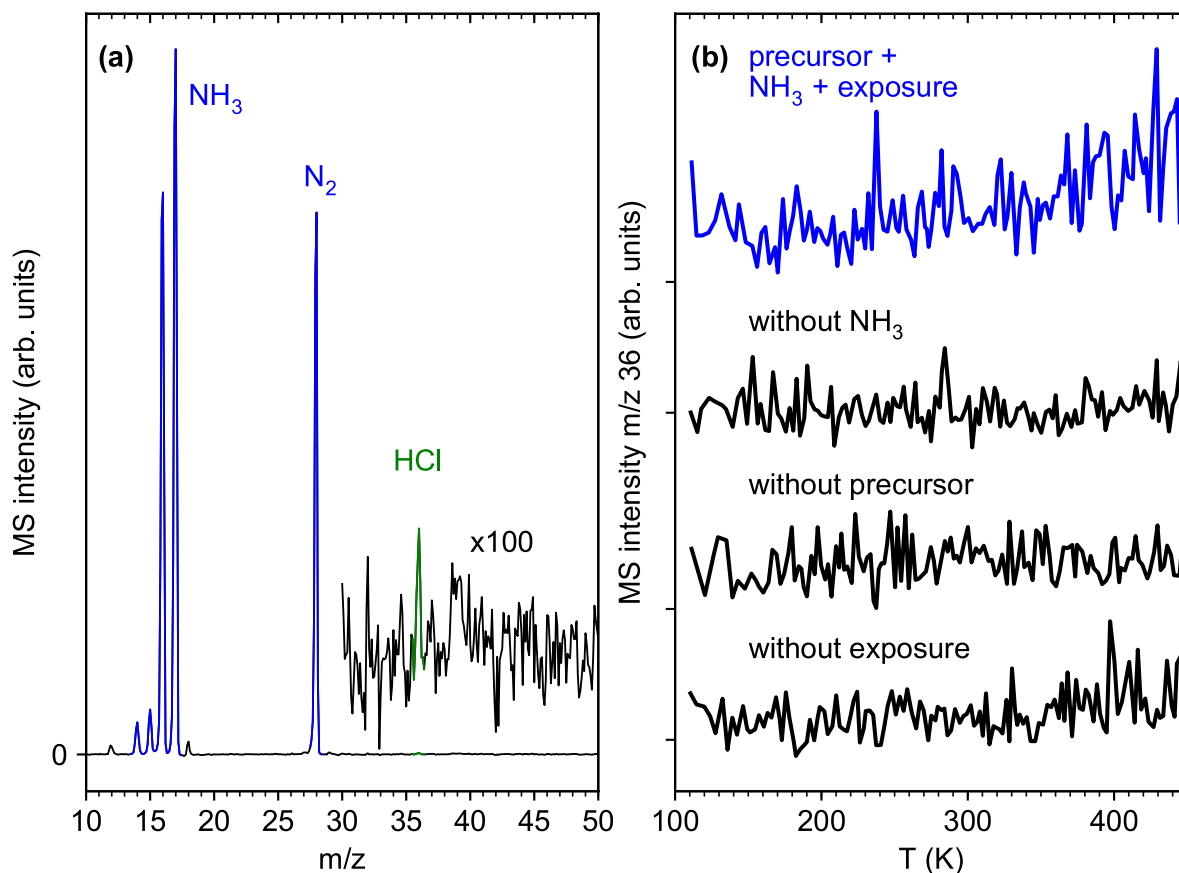
Figure 6. Auger electron spectra (AES) recorded on a deposit prepared by electron exposure ($1.25 \cdot 10^{17}$ e$^-$/cm^2) at $E_0 = 31$ eV and subsequent annealing to 450 K of an adsorbed layer of (η^3-C$_3$H$_5$)Ru(CO)$_3$Cl on Ta before (bottom) and after an increasing number of purification cycles (from bottom to top) **(a)** in the presence of NH$_3$ and **(b)** without NH$_3$. Each purification cycle comprised an electron exposure of $1.25 \cdot 10^{16}$ e$^-$/cm^2 followed by annealing to 450 K. **(c)** Relative amounts of Cl and Ru after increasing numbers of purification cycles performed on the deposit in presence of NH$_3$ (blue) and on the deposit only (black). These values were determined from the peak-to-peak intensities of the Cl signal at 184 eV and the Ru signal at 235 eV by accounting for the respective sensitivity factors for 5 keV impinging electrons [0.6941 for Ru (235 eV) and 8.1285 for Cl (184 eV)[28]].

by annealing to 450 K during a further TDS run (see Fig. 1f). AES was performed with the sample held at room temperature prior to the first cycle and after selected purification cycles (Fig. 6a). For comparison, the same sequence of experiments was performed without condensing NH$_3$ on the deposit (Fig. 6b). It is obvious that the Cl content decreases more rapidly in the presence of NH$_3$. This was quantified by evaluating the intensity of the Cl and Ru signals. Unfortunately, the more sensitive Ru Auger signal at 277 eV coincides closely with the C signal at 275 eV and can therefore not be used. Therefore, the relative intensities of the Cl signal (184 eV) and the smaller Ru signal at 235 eV have been determined from the AES data for purification experiments with and without NH$_3$ (Fig. 6c). We note that the ratio Cl:Ru was roughly 0.6 already prior to the first purification cycle. Considering that only minor desorption of Cl was detected during deposit formation, a ratio near one would have been expected. However, a precise quantitative analysis of AES data requires careful evaluation of effects from background corrections, instrumental resolution, backscattered electrons, and layer structure of the sample[27,28]. Such a precise analysis is beyond the scope of the present work.

Note that some loss of Cl is also expected under the 5 keV AES electron beam[14]. Therefore, each AES was acquired on a new spot of the sample. The systematic decrease of the Cl signal with increasing number of purification cycles (Fig. 6a,c) thus results from the combined effects of electron irradiation at 31 eV in the presence of NH$_3$ and the subsequent annealing step. In consequence, Fig. 6c clearly supports that the electron-induced removal of Cl from a deposit produced from (η^3-C$_3$H$_5$)Ru(CO)$_3$Cl is enhanced by the presence of NH$_3$.

The AES data (Fig. 6a,b) also reveal the presence of nitrogen (389 eV) and oxygen (510 eV). In particular, the amount of surface-bound N keeps increasing with the number of purification cycles giving evidence of a reaction between NH$_3$ and the surface. The AES signal of N was also observed when the purification cycles were applied to the clean Ta substrate (Supplementary Information, Fig. S5), indicating that N becomes chemically bonded to the underlying substrate. However, chemisorption of atomic N on Ru surfaces can occur[29,30] so that a reaction with small Ru aggregates that emerge during purification of the deposit is also conceivable. The O Auger signal in Fig. 5 and Fig. S5 can be traced back to residual H$_2$O in the vacuum chamber that reacts with the Ta surface (Supplementary Information, Fig. S6) and possibly also with the emerging metallic Ru[31]. Note that the different intensity of O in Fig. 5a and b relates to the time between the sputtering process and the purification experiment.

Figure 7. (**a**) Accumulated mass spectrum acquired during an electron exposure of $1.25 \cdot 10^{16}$ e$^-$/cm^2 at $E_0 = 31$ eV of the first deposit purification cycle in the presence of NH$_3$ at 110 K as shown in Fig. 5a. Note a very small signal at m/z 36 that points to desorption of small amounts of HCl. (**b**) Thermal desorption spectra (TDS) acquired at m/z 36 following this electron irradiation as well as control experiments performed either without NH$_3$, without prior electron exposure, and also without a precursor layer. Desorption of HCl occurs only when electron irradiation of the deposit is performed in the presence of NH$_3$.

This was longer in Fig. 5a where sputtering and purification were performed on different days. However, the amount of H$_2$O accumulated during the time span of deposit fabrication is very small as compared to NH$_3$ applied during the purification cycles (Supplementary Information, Fig. S7) Therefore, the effect of H$_2$O on the deposit purification chemistry can be neglected.

Electron-stimulated desorption during deposit purification in presence of NH$_3$. Unfortunately, the amounts of Cl and HCl are difficult to assess in a quantitative manner from the present ESD and TDS results, which raises questions about the fate of Cl during the purification steps. While ESD of HCl from cisplatin (*cis*-Pt(NH$_3$)$_2$Cl$_2$) was clearly seen at $E_0 = 500$ eV and room temperature[16], electron irradiation during the present purification cycles was performed at 110 K and thus much below the desorption temperature of HCl (Fig. 2). However, accumulated mass scans performed during electron irradiation within the first purification cycle of Fig. 6a show a tiny signal of HCl at m/z 36 beside the strong desorption of NH$_3$ and of its decomposition product N$_2$ (Fig. 7a, experiment visualized in Fig. 1e). Furthermore, the TDS experiment performed at m/z 36 after the electron exposure of $1.25 \cdot 10^{16}$ e$^-$/cm^2 also shows a small desorption signal with onset at 350 K (Fig. 7b, experiment visualized in Fig. 1e), despite the fact that this exposure was ten times smaller than that applied for deposit formation. This signal has not reached its maximum at 450 K, suggesting that more HCl must have desorbed during the subsequent bakeout period at 450 K (see "Methods").

We note that NH$_4$Cl was identified by RAIRS as an intermediate product of the electron-induced decomposition of cisplatin[16]. NH$_4$Cl decomposes thermally only above 450 K[32] and might, in consequence, trap Cl until further electron exposure at 5 keV during AES. Therefore, RAIRS was performed in a separate experiment before the first purification cycle, after electron exposure, and after annealing during TDS (Supplementary Information, Fig. S8). However, the signal of NH$_4$Cl was absent so that formation of such a less volatile product is not responsible for the relatively low apparent yield of HCl during ESD and TDS.

Discussion

The aim of this study was to assess the potential of NH_3 to assist in the removal of Cl during electron-induced deposit formation from a thin adsorbate of $(\eta^3\text{-}C_3H_5)Ru(CO)_3Cl$ or in a post-deposition purification process. AES shows that the presence of NH_3 in fact enhances the removal of Cl from a model deposit (Fig. 6). After a total exposure of $3.1 \cdot 10^{17}$ e⁻/cm² at 31 eV in the presence of coadsorbed NH_3 with intermittent annealing to 450 K, the Cl content has been reduced by roughly 75%. The same procedure performed without NH_3 leads to a smaller reduction of approximately 40%.

We compare the observed loss of Cl to previous results for layers of $(\eta^3\text{-}C_3H_5)Ru(CO)_3Br$ and $(\eta^3\text{-}C_3H_5)Ru(CO)_3Cl$ at 105 K and with similar thickness as used here but for exposure at 500 eV[14]. Both compounds decompose with a very similar rate under electron exposure. For $(\eta^3\text{-}C_3H_5)Ru(CO)_3Cl$, longer exposures were not reported but the halide content was reduced by less than 10% after an exposure of $7.58 \cdot 10^{16}$ e⁻/cm² in close agreement to $(\eta^3\text{-}C_3H_5)Ru(CO)_3Br$[14]. The bromide complex can therefore also serve as reference. In particular, the Br content was reduced by roughly 35% after an electron exposure of $5.63 \cdot 10^{17}$ e⁻/cm²[14]. This is close to the reduction of the Cl content by the present purification cycles in the absence of NH_3. Note here that thermal processing can contribute to removal of Cl in our experiment so that the result does not allow us to directly compare the efficiency of the underlying electron-induced chemistry at 31 eV to that reported for 500 eV[14]. However, halide removal was obviously slower in the previous purification attempts by electron irradiation alone[14] than in our present NH_3-based process.

The previous study also explored the room temperature purification of a deposit produced at the same temperature in a FEBID-type process from $(\eta^3\text{-}C_3H_5)Ru(CO)_3Cl$[14]. AES revealed that the Cl content dropped to about 25% of its initial value during a post-deposition electron exposure of $7.9 \cdot 10^{18}$ e⁻/cm² at 3 keV. This is again slower than in the present NH_3-based process where an electron exposure that was more than an order of magnitude smaller has achieved a similar effect. A more detailed comparison between these two experiments is difficult because the previous study did not report the thickness of the deposit[14]. However, we estimate that the electron beam fully penetrated the deposit because the signal of the underlying Ag substrate was still visible.

This enhancing effect of NH_3 is similar to the case of cisplatin (cis-Pt(NH₃)₂Cl₂) studied previously[16,17]. In particular, electron exposure removed Cl more rapidly from cisplatin than from the analogous precursor cis-Pt(CO)₂Cl₂, that was studied earlier under similar conditions[33]. It was proposed[16] that electron impact ionization of NH_3 triggers proton transfer to Cl⁻ (Eq. 1).

$$NH_3^+ + Cl^- \rightarrow HCl + NH_2^{\cdot} \tag{1}$$

Also, electron-induced fragmentation yielding NH_x (x < 3) leads to release of atomic hydrogen (AH) that can react with the Cl ligand (Eq. 2).

$$H^{\cdot} + Pt - Cl \rightarrow HCl + Pt \tag{2}$$

Both reactions (1) and (2) yield HCl as observed in ESD from cisplatin[16]. Note again that the desorption efficiency of HCl was presumably higher for cisplatin than for $(\eta^3\text{-}C_3H_5)Ru(CO)_3Cl$ studied here because ESD was performed at room temperature and higher E_0. However, the electron-induced decomposition of cisplatin was very slow and ESD of HCl not visible when E_0 was decreased to 50 eV. This underlines again that the close similarity between the decomposition rate of $(\eta^3\text{-}C_3H_5)Ru(CO)_3Cl$ at 500 eV as reported before[14] and at 31 eV as studied herein is unexpected and should be studied in more detail.

Fundamental insight into the electron-induced fragmentation of $(\eta^3\text{-}C_3H_5)Ru(CO)_3X$ precursors via dissociative electron attachment (DEA) and dissociative ionization (DI) may point to an explanation for the unexpectedly high electron-induced decomposition rate of $(\eta^3\text{-}C_3H_5)Ru(CO)_3Cl$ at 31 eV. In the case of $(\eta^3\text{-}C_3H_5)Ru(CO)_3Br$, DI leads to more comprehensive loss of ligands than DEA[13]. If DI is equally dominant for the Cl analogue, the cross section of the electron-induced fragmentation at 31 eV can be comparable or even higher than at 500 eV. This is suggested by comparison with the electron energy dependence of DI from Co(CO)₃NO[34]. If, on the other hand, DEA was the dominant process, the larger yield of SEs at 500 eV should enhance the reactions as compared to lower E_0. This latter kind of reactivity was held responsible for the much faster decomposition of cisplatin at 500 eV as compared to 50 eV[16]. However, absolute cross sections for DEA and DI would be needed to further support this interpretation.

Our attempts to enhance the electron-induced release of HCl by adsorbing NH_3 on the pristine layer of $(\eta^3\text{-}C_3H_5)Ru(CO)_3Cl$ prior to exposure were not successful. A possible reason is that NH_3 interacts only weakly with the intact precursor layer. In fact, the present experiments were performed close to the multilayer desorption temperature of NH_3[19]. Also, ESD of NH_3 is already efficient at 35 K and 15 eV[19] and obvious in the present experiments from the mass spectrum acquired during electron irradiation of the first deposit purification cycle (Fig. 7a), and from the nearly quantitative loss of NH_3 vibrational bands in RAIRS after this irradiation (Supplementary Information, Fig. S8). In contrast to cisplatin where NH_3 is directly bonded to the central metal atom in direct vicinity to the Cl ligands, the crowded coordination sphere of intact $(\eta^3\text{-}C_3H_5)Ru(CO)_3Cl$ probably shields the Cl ligand from the weakly physisorbed NH_3. In consequence, physisorbed NH_3 molecules do not contribute noticeably to the decomposition of $(\eta^3\text{-}C_3H_5)Ru(CO)_3Cl$ and removal of Cl. In contrast, the deposit produced by electron irradiation is depleted of CO so that coordination sites on the Ru center are more easily accessible to NH_3, enabling a close approach to the Cl ligand. We thus propose that NH_3 can coordinate to the Ru center of the precursor after some CO ligands have been removed by electron irradiation. This enhances the probability that electron irradiation ionizes or fragments NH_3 near the Cl ligand which can consequently induce the formation of HCl, most likely in an intramolecular reaction.

The combination of ESD experiments at cryogenic temperature with TDS allow us to identify potential contributions of thermal reactions to the decomposition of $(\eta^3\text{-}C_3H_5)Ru(CO)_3Cl$ under FEBID-type conditions,

where the precursor is irradiated at or above room temperature[10]. In fact, the ESD and TDS results (Figs. 2, 3) show that roughly 10% of the CO ligands remain within the deposit at cryogenic temperature after irradiation but are removed by increasing the temperature to 450 K. Also, small amounts of C_3 hydrocarbons, presumably formed through electron-induced reactions involving H transfer between two allyl ligands, desorb during electron exposure (Fig. 2). Additional propene and HCl desorb during the temperature increase (Fig. 3). However, our rough estimate of the quantities of these products demonstrates that these reactions are of minor relevance. This rationalizes why most of the carbon content and all of the Br ligands remain in the deposit when FEBID is performed with $(\eta^3\text{-}C_3H_5)Ru(CO)_3Br$[14,15]. Additionally, we note that desorption of C_3 hydrocarbons was not seen during deposit purification (Fig. 7a). We therefore conclude that NH_3 is a suitable reagent to enhance the removal of Cl and possibly of other halides but is not beneficial with respect to removal of carbon.

Conclusion

NH_3 present during post-deposition electron irradiation enhances the removal of Cl from deposits produced by electron-induced decomposition of $(\eta^3\text{-}C_3H_5)Ru(CO)_3Cl$. Intramolecular reactions of the Cl ligands with NH_3 adsorbed on coordination sites of Ru that were liberated by electron-induced and thermal loss of CO are held responsible for this enhancement. In contrast, thermal reactions contribute to the desorption of CO but remove only minor amounts of the allyl and Cl ligands.

Methods

Precursor synthesis.   Synthesis was carried out under an inert atmosphere (N_2) using standard Schlenk techniques. Reagents were purchased from Acros Organics, Oakwood Chemical, and Fisher Scientific and used without further purification. ^{1}H NMR spectra (Supplementary Information, Fig. S9) were obtained on a 400 MHz Bruker spectrometer and signals were referenced to the residual protons of $CDCl_3$. IR Spectroscopy (Supplementary Information, Fig. S10) was performed on a Perkin Elmer Spectrum One Fourier transform infrared spectrometer using a solution cell equipped with NaCl windows and a path length of 1.0 mm. Synthesis and purification of $(\eta^3\text{-}C_3H_5)Ru(CO)_3Cl$ was carried out using a literature procedure[35]. The compound was characterized by comparison to literature data[35]. 1H NMR (300 MHz, $CDCl_3$) δ 5.29 (tt, 1H, J = 8.7, 13.2 Hz), 4.20 (dd, 2H, J = 8.7, 1.0 Hz), 2.98 (dd, 2H, J = 13.2, 1.0 Hz). IR (heptane) 2,111, 2,062, 2,016 cm^{-1}.

The integrity of the compound after shipping to Bremen was checked up to a sublimation temperature of 200 °C by EI-MS which shows the parent ion as well as the characteristic series of ligand losses (Supplementary Information, Fig. S11).

UHV setup.   All experiments were performed in an ultrahigh vacuum (UHV) setup described previously[10, 36] with a base pressure of about 10^{-10} mbar. It contains a polycrystalline Ta sheet held at 110 K by liquid N_2 cooling. The sample temperature is controlled by resistive heating of two thin Ta ribbons spot-welded to the thicker Ta sheet and is measured using a type E thermocouple press-fitted to the Ta substrate. The setup is equipped with a quadrupole mass spectrometer (QMS) residual gas analyser (Stanford, 300 amu) with electron impact ionization at 70 eV, a commercial flood gun (SPECS FG 15/40) for electron irradiation, an Auger electron spectrometer (STAIB DESA 100), and a sputter gun operated with Ar$^+$ ions. All Auger electron spectra (AES) were recorded using an electron energy of 5 keV.

Preparation of adsorbed layers and estimate of thickness.   Sample preparation was performed in line with previously reported procedures[10]. Prior to an experiment, the substrate was sputter-cleaned using Ar$^+$ ions at 3 keV until the AES signals of the underlying Ta were clearly visible and any other signals, in particular, remaining Ru and C signals had disappeared. Immediately before each precursor deposition, adsorbed volatile compounds from the residual gas were further removed by annealing to 450 K through resistive heating of two thin Ta ribbons spot-welded to the thicker Ta sheet. The precursor $(\eta^3\text{-}C_3H_5)Ru(CO)_3Cl$ was condensed on the Ta sheet at 110 K. This was done by introducing the precursor via a gas handling manifold consisting of precision leak valves and a small calibrated volume where the absolute pressure is measured with a capacitance manometer. For each film deposition, a calibrated amount of vapour was leaked via a stainless steel capillary opening onto the Ta substrate. However, due to slow decomposition of the precursor within the reservoir, this vapour contained some CO and a hydrocarbon species deriving from the allyl ligand. Therefore, a pumping cycle was applied to the reservoir prior to each dosing of the precursor. Also, the substrate was heated to a temperature of 170 K after each introduction of vapour to remove any free ligands from the layer of $(\eta^3\text{-}C_3H_5)Ru(CO)_3Cl$ which starts to desorb at a temperature around 200 K.

The desorption temperature of $(\eta^3\text{-}C_3H_5)Ru(CO)_3Cl$ as well as the film thickness were estimated by thermal desorption spectrometry (TDS) performed after introducing varying amounts of vapour. The QMS was used to monitor desorbing species during application of a temperature ramp of 1 K/s to the sample. The data recorded at m/z 41 (Supplementary Information, Fig. S2) show a weak desorption signal with maximum around 240 K which rapidly saturates when the pressure drop in the manifold was increased to 2 mTorr and is therefore ascribed to the monolayer. A second peak with maximum at 220 K starts to increase upon saturation of the monolayer peak, i.e., when larger pressure drops were noted in the manifold, and is hence attributed to the successive layers no longer in contact with the substrate. All further experiments were performed on precursor layers produced by leaking an amount of vapour corresponding to a pressure drop of 5 mTorr in the manifold. According to our estimate, this yielded a 2–3 monolayer adsorbate of the precursor. Assuming that the molecular size of $(\eta^3\text{-}C_3H_5)Ru(CO)_3Cl$ is roughly comparable to that of $MeCpPtMe_3$ for which an effective diameter of 0.96 nm has been deduced[37], 2–3 monolayers would result in an average thickness of 2–3 nm, similar to the thickness used previously[14]. However, it was noted from TDS data acquired from pristine precursor layers prior to the experiments reported herein that

an additional desorption signal at higher temperature was occasionally present (Supplementary Information, Fig. S4). Considering the observed release of ligands and, in particular, CO from the precursor in the reservoir, this signal is most likely ascribed to an unknown volatile decomposition product. Therefore, the absolute amount of $(\eta^3\text{-}C_3H_5)Ru(CO)_3Cl$ in the adsorbed layers varied somewhat with time.

For purification experiments, NH_3 was leaked onto the substrate held at 110 K. Again, TDS performed after leaking varying amounts of NH_3 vapour onto the Ta substrate revealed that the surface coverage increased with increasing pressure drop in the manifold (Supplementary Information, Fig. S12). As 110 K is close to the multilayer desorption temperature of NH_3[21], the desorption signals increase sharply at the onset of the temperature ramp. Therefore, the TDS data for NH_3 do not allow us to safely identify the transition from monolayer to multilayer regime. NH_3 adsorbates in all further experiments were prepared by leaking an amount of vapour corresponding to a pressure drop of 5 mTorr in the manifold. We assume that consequently, during each experiment, NH_3 was present on the substrate with a coverage at least within the monolayer regime.

Electron-induced degradation of $(\eta^3\text{-}C_3H_5)Ru(CO)_3Cl$.

The electron-induced degradation of the $(\eta^3\text{-}C_3H_5)Ru(CO)_3Cl$ layers was studied by electron-stimulated desorption (ESD) isothermal experiments as well as by subsequent TDS in line with a methodology described previously[10]. For ESD, the sample was kept at 110 K and exposed to electron irradiation from the flood gun. This electron source delivers electrons with tuneable kinetic energy (E_0) at an estimated resolution of the order of 0.5–1 eV. Here, E_0 was set to 31 eV in all experiments, resulting in currents as measured at the substrate (I_p) of the order of up to 150 μA for an irradiated area of 5 cm^2. All ESD data were corrected by the background spectrum of residual gases. In the case that a mass spectrum was acquired during ESD, the background mass spectrum of the UHV chamber as measured immediately before starting the irradiation was subtracted. In experiments that monitored specific m/z ratios during electron exposure, the intensity levels before the start of irradiation and after its end were used to define a linear baseline to be subtracted.

After each electron irradiation, a TDS experiment was performed by applying a temperature ramp up to 450 K with a heating rate of 1 K/s to monitor products that desorb thermally from the degraded precursor layer. Subsequently, the sample was held at 450 K for typically 30 s to remove further volatile substances (bakeout). In each TDS, the signals of up to four selected characteristic masses were recorded. To evaluate the effect of NH_3 on the electron-induced decomposition of the precursor, NH_3 was dosed onto a layer of $(\eta^3\text{-}C_3H_5)Ru(CO)_3Cl$. After this preparation, ESD and subsequent TDS were again performed.

Purification experiments.

For purification experiments, a deposit was produced by performing electron irradiation on an adsorbed layer of $(\eta^3\text{-}C_3H_5)Ru(CO)_3Cl$ followed by annealing to 450 K in a TDS experiment and subsequent bakeout. The cryostat was then allowed to warm up to room temperature for AES analysis. Subsequently, the substrate was again cooled to 110 K followed by condensation of NH_3 on the deposit. The sample was then subjected to electron irradiation to an exposure of 2000 μC/cm^2 ($1.25 \cdot 10^{16}$ e$^-$/cm^2) at $E_0 = 31$ eV, followed by a further TDS run applying annealing to 450 K. This purification cycle was repeatedly applied. The elemental composition after selected purification cycles was monitored again by AES at room temperature. Each AES was acquired on a new spot of the sample to exclude contributions of the high-energy electron gun of the Auger spectrometer to the changes in composition. In a control experiment with the same sequence of cycles, the effect of irradiation in the absence of NH_3 was studied.

In addition, electron-induced reactions of NH_3 with the underlying Ta substrate in the absence of precursor were also monitored (Supplementary Information, Fig. S5). Finally, oxygen signals that showed up in the AES data were traced back to oxidation of the Ta substrate by residual H_2O in the vacuum chamber (Supplementary Information, Fig. S6). However, comparison of TDS curves acquired from an NH_3 adsorbate layer and on the clean Ta substrate after a waiting time corresponding to an entire ESD and TDS cycle revealed that the contribution of H_2O to the electron-induced precursor decomposition must be negligible (Supplementary Information, Fig. S7).

Data availability
The data sets generated during and/or analysed during the current study are available from the corresponding author upon reasonable request.

References

1. Utke, I., Hoffmann, P. & Melngailis, J. Gas-assisted focused electron beam and ion beam processing and fabrication. *J. Vac. Sci. Technol. B* **26**, 1197–1276 (2008).
2. Huth, M., Porrati, F. & Dobrovolskiy, O. V. Focused electron beam induced deposition meets materials science. *Microelectron. Eng.* **185–186**, 9–28 (2018).
3. Winkler, R. *et al.* Direct-write 3d nanoprinting of plasmonic structures. *ACS Appl. Mater. Interfaces* **9**, 8233–8240 (2017).
4. Swiderek, P., Marbach, H. & Hagen, C. W. Chemistry for electron-induced nanofabrication. *Beilstein J. Nanotechnol.* **9**, 1317–1320 (2018).
5. Botman, A., Mulders, J. J. L. & Hagen, C. W. Creating pure nanostructures from electron-beam-induced deposition using purification techniques: A technology perspective. *Nanotechnology* **20**, 372001 (2009).
6. Wnuk, J. D. *et al.* Electron induced surface reactions of the organometallic precursor trimethyl(methylcyclopentadienyl) platinum(IV). *J. Phys. Chem. C* **113**, 2487–2496 (2009).
7. Thorman, R. M., Ragesh, K. T., Fairbrother, D. H. & Ingólfsson, O. The role of low-energy electrons in focused electron beam induced deposition: Four case studies of representative precursors. *Beilstein J. Nanotechnol.* **6**, 1904–1926 (2015).

8. Geier, B. *et al.* Rapid and highly compact purification for focused electron beam induced deposits: A low temperature approach using electron stimulated H_2O reactions. *J. Phys. Chem. C* **118**, 14009–14016 (2014).
9. Shawrav, M. M. *et al.* Highly conductive and pure gold nanostructures grown by electron beam induced deposition. *Sci. Rep.* **6**, 34003 (2016).
10. Warneke, Z., Rohdenburg, M., Warneke, J., Kopyra, J. & Swiderek, P. Electron-driven and thermal chemistry during water-assisted purification of platinum nanomaterials generated by electron beam induced deposition. *Beilstein J. Nanotechnol.* **9**, 77–90 (2018).
11. Noh, J. H. *et al.* Nanoscale electron beam-induced deposition and purification of ruthenium for extreme ultraviolet lithography mask repair. *Appl. Phys. A* **117**, 1705–1713 (2014).
12. Edinger, K. *et al.* Electron-beam-based photomask repair. *J. Vac. Sci. Technol. B Microelectron. Nanom. Struct. Process. Meas. Phenom.* **22**, 2902–2906 (2004).
13. Thorman, R. M., Brannaka, J. A., McElwee-White, L. & Ingólfsson, O. Low energy electron-induced decomposition of (η^3-C_3H_5) $Ru(CO)_3Br$, a potential focused electron beam induced deposition precursor with a heteroleptic ligand set. *Phys. Chem. Chem. Phys.* **19**, 13264–13271 (2017).
14. Spencer, J. A., Brannaka, J. A., Barclay, M., McElwee-White, L. & Fairbrother, D. H. Electron-induced surface reactions of η^3-allyl ruthenium tricarbonyl bromide [(η^3-C_3H_5)$Ru(CO)_3Br$]: Contrasting the behavior of different ligands. *J. Phys. Chem. C* **119**, 15349–15359 (2015).
15. Jurczyk, J. *et al.* Focused electron beam-induced deposition and post-growth purification using the heteroleptic Ru complex (η^3-C_3H_5)$Ru(CO)_3Br$. *ACS Appl. Mater. Interfaces* **11**, 28164–28171 (2019).
16. Rohdenburg, M. *et al.* Cisplatin as potential Pt FEBID precursor: NH_3 ligands enhance the electron-induced removal of chlorine. *J. Phys. Chem. C* **123**, 21774–21787 (2019).
17. Warneke, J. *et al.* Role of NH_3 in the electron-induced reactions of adsorbed and solid cisplatin. *J. Phys. Chem. C* **120**, 4112–4120 (2016).
18. Madey, T. E. Electron- and photon-stimulated desorption: Probes of structure and bonding at surfaces. *Science* **234**, 316–322 (1986).
19. Wallace, W.E., Mass spectra by NIST mass spectrometry data center. In *NIST Chemistry WebBook* (Linstrom, P. J., Mallard, W. G. Eds.) NIST Standard Reference Database Number 69. National Institute of Standards and Technology, Gaithersburg. https://webbook.nist.gov. Retrieved 24 Sept 2019.
20. Walker, C. G. H., El-Gomati, M. M., Assa'd, A. M. D. & Zaradžil, M. The secondary electron emission yield for 24 solid elements excited by primary electrons in the range 250–5000 eV: A theory/experiment comparison. *Scanning* **30**, 365–380 (2008).
21. Böhler, E., Bredehöft, J. H. & Swiderek, P. Low-energy electron-induced hydroamination reactions between different amines and olefins. *J. Phys. Chem. C* **118**, 6922–6933 (2014).
22. Daschbach, J. L., Kim, J., Ayotte, P., Smith, R. S. & Kay, B. D. Adsorption and desorption of HCl on Pt(111). *J. Phys. Chem. B* **109**, 15506–15514 (2005).
23. Elam, J. W., Nelson, C. E., Tolbert, M. A. & George, S. M. Adsorption and desorption of HCl on a single-crystal α-Al2O3(0001) surface. *Surf. Sci.* **450**, 64–77 (2000).
24. Kim, M. A. *et al. Electron-Impact Cross Sections for Ionization and Excitation Database, NIST Standard Reference Database 107.* https://physics.nist.gov/ionxsec. Accessed 28 Aug 2019.
25. Ali, M. A. & Kim, Y.-K. Ionization cross sections by electron impact on halogen atoms, diatomic halogen and hydrogen halide molecules. *J. Phys. B At. Mol. Opt. Phys.* **41**, 145202 (2008).
26. Thussing, S., Gazdzicki, P. & Jakob, P. Adsorption of CO on bimetallic RhN/Ru(0001) layers. *Surf. Sci.* **623**, 29–40 (2014).
27. Shimizu, R. Quantitative analysis by Auger electron spectroscopy. *Jpn. J. Appl. Phys.* **22**, 1631–1642 (1983).
28. Seah, M. P. Quantification in AES and XPS. In *Surface Analysis by Auger and X-ray Photoelectron Spectroscopy* (eds. Briggs, D. & Grant, J. T.) 345–375 (IM Publications, Chichester/Surface Spectra, Manchester, 2003).
29. Jacobi, K. Nitrogen on ruthenium single-crystal surfaces. *Phys. Stat. Sol. (A)* **177**, 37–51 (2000).
30. Danielson, L. R., Dressler, M. J., Donaldson, E. E. & Sandstrom, D. R. Effects of an electron beam on adsorption and desorption of ammonia on ruthenium (0001). *Surf. Sci.* **71**, 615–629 (1978).
31. Madey, T. E., Faradzhev, N. S., Yakshinskiy, B. V. & Edwards, N. V. Surface phenomena related to mirror degradation in extreme ultraviolet (EUV) lithography. *Appl. Surf. Sci.* **253**, 1691–1708 (2006).
32. Olszak-Humienik, M. On the thermal stability of some ammonium salts. *Thermochim. Acta* **378**, 107–112 (2001).
33. Spencer, J. A., Wu, Y.-C., McElwee-White, L. & Fairbrother, D. H. Electron induced surface reactions of cis-$Pt(CO)_2Cl_2$: A route to focused electron beam induced deposition of pure Pt nanostructures. *J. Am. Chem. Soc.* **138**, 9172–9182 (2016).
34. Engmann, S. *et al.* Absolute cross sections for dissociative electron attachment and dissociative ionization of cobalt tricarbonyl nitrosyl in the energy range from 0 eV to 140 eV. *J. Chem. Phys.* **138**, 044305 (2013).
35. Brewer, C. R. *et al.* Photochemistry of (η^3-allyl)$Ru(CO)_3X$ precursors for photoassisted chemical vapor deposition. *Organometallics* **38**, 4363–4370 (2019).
36. Ipolyi, I., Michaelis, W. & Swiderek, P. Electron-induced reactions in condensed films of acetonitrile and ethane. *Phys. Chem. Chem. Phys.* **9**, 180–191 (2007).
37. Xue, Z. *et al.* Characterization of (methylcyclopentadienyl)trimethylplatinum and low-temperature organometallic chemical vapor deposition of platinum metal. *J. Am. Chem. Soc.* **111**, 8779–8784 (1989).

Acknowledgements

Author contributions

All authors discussed the organization and content of the manuscript. MR devised the experiments, participated in the acquisition and analysis of the data, prepared the final figures, and revised the manuscript. HB carried out most of the experiments, analysed the data, and prepared the initial versions of the figures. CRB synthesized the precursor and revised the manuscript. LMW revised the manuscript. PS wrote the manuscript.

Competing interests

The authors declare no competing interests.

Additional information

Supplementary information is available for this paper at https://doi.org/10.1038/s41598-020-67803-y.

Correspondence and requests for materials should be addressed to M.R. or P.S.

Reprints and permissions information is available at www.nature.com/reprints.

Publisher's note Springer Nature remains neutral with regard to jurisdictional claims in published maps and institutional affiliations.